Eur. Phys. J. Plus (2018) **133**: 154
DOI 10.1140/epjp/i2018-11991-2

THE EUROPEAN PHYSICAL JOURNAL PLUS

Regular Article

Numerical study of unsteady Williamson fluid flow and heat transfer in the presence of MHD through a permeable stretching surface

Madiha Bibi[1], Khalil-Ur-Rehman[1,a], M.Y. Malik[1,2], and M. Tahir[3]

[1] Department of Mathematics, Quaid-i-Azam University, Islamabad 44000, Pakistan
[2] Department of Mathematics, Faculty of Science, King Abdulaziz University, PO Box-80203, Jeddah 21589, Saudi Arabia
[3] Department of Mathematics, Faculty of Basic Sciences, HITEC University, Taxila, Pakistan

Received: 5 May 2017 / Revised: 17 January 2018
Published online: 20 April 2018 –

Abstract. In the present article, unsteady flow field characteristics of the Williamson fluid model are explored. The nanosized particles are suspended in the flow regime having the interaction of a magnetic field. The fluid flow is induced due to a stretching permeable surface. The flow model is controlled through coupled partial differential equations to the used shooting method for a numerical solution. The obtained partial differential equations are converted into ordinary differential equations as an initial value problem. The shooting method is used to find a numerical solution. The mathematical modeling yields physical parameters, namely the Weissenberg number, the Prandtl number, the unsteadiness parameter, the magnetic parameter, the mass transfer parameter, the Lewis number, the thermophoresis parameter and Brownian parameters. It is found that the Williamson fluid velocity, temperature and nanoparticles concentration are a decreasing function of the unsteadiness parameter.

1 Introduction

The magnetohydrodynamics generators, geothermal energy extractions, nuclear reactors, and the plasma studies are the few pertinent applications of heat transfer along with magnetic field interaction subject to boundary layer flows. Therefore, various attempts are reported on magnetohydrodynamics namely, Damseh [1] discussed the influence of a magnetic field on boundary layer flow due to an exponentially stretching surface. The MHD viscoelastic fluid flow induced by a stretching flat surface was considered by Abel and Nandeppanavar [2]. The impact of a magnetic filed on unsteady flow via a shrinking surface was investigated by Merkin and Kumaran [3]. In the presence of heat source/sink and thermal radiation effects the MHD viscoelastic fluid flow was studied by Nandeppanavar *et al.* [4]. Since then a lot of work is given by prolific researchers to highlight the importance of magnetic field effects on boundary layer flow induced by different stretching surfaces. One can assess the past and recent developments in this regard in refs. [5–14].

A vast classification of non-Newtonian fluids is based upon their characteristics and the physical factors. Time-dependent fluids class is one of the major classes. Heat and mass flow is effected with the change in time that is why the study of unsteady flows has great importance in industrial applications. From a historical point of view a classical paper was given by Stewartson [15], in which he has given the concept of unsteady laminar boundary layer for the very first time. Perepelitza [16] investigated the unsteady heat transfer and gave the experimental results that stabilized heat transfer at Reynolds numbers of $(0.8–6.8) \times 10^4$ for $5\,\text{mm} \times 40\,\text{mm}$, $10\,\text{mm} \times 40\,\text{mm}$, and $20\,\text{mm} \times 40\,\text{mm}$ channels. Recently Bachok *et al.* [17] compared the time-dependent boundary layer of heat and mass flow over a permeable stretching sheet for two different solutions. Rees *et al.* [18] investigated the time-dependent thermal boundary layer for the Bingham fluid in the porous medium, they concluded that the fluid stayed stagnant at early times because the resulting buoyancy forces were too weak to overcome the yield threshold.

[a] e-mail: krehman@math.qau.edu.pk

In industry the pseudoplastic fluids have great importance, specially in the chemical and petroleum industry. The Williamson fluid also drops in the pseudoplastic class of fluids. This model was introduced by Williamson [19] in 1929 and he gave the experimental results. Although this model gained little attention by the researchers, in the last decade Dapra and Scarpi [20] gave the perturbation method for Williamson fluid flow in fractured rock and Khan *et al.* [21] gave the Homotopy Analysis Method (HAM) for the Williamson fluid reaction with other chemicals. A most recent study of this model was done by Hayat [22] and Malik *et al.* [23]. Rehman *et al.* [24] analyzed the double stratification and chemically reactive species for the Williamson fluid numerically and concluded that the thermal stratification depreciate the velocity and heat of the fluid. Rehman *et al.* [25] also discussed the mixed convection under the stagnation region over an inclined cylindrical surface.

In the current article the Williamson fluid is taken as a base fluid and nano paricles are used to enhance the heat flow rate. The word "nanofluid" was firstly used by Choi and Eastman [26] to allude to the scattering of nano-particles in the base fluid for the enhancement of thermal conductivities. He had unwrapped a field of study which is of great importance in the industry because nanofluids play a magical role as coolants for many industrial and automotive purposes. Nandy and Mahapatra [27] investigated the effect of nano particles in the presence of MHD. The latest numerical model for the cooling performance of exhaust gas recirculation (EGR) cooler by using nanofluids is given by Shabgard *et al.* [28].

A stretching surface is mostly the cause of flow in most of industrial applications, like hot rolling, extrusion of metals and plastic. Crane [29] was the first one who studied the flow past a stretching surface. Then Wang [30] and Fang *et al.* [31] started the study of a shrinking sheet. After some time Ishak *et al.* [32] contemplated the boundary layer flow of mass and heat of nano fluid past a porous shrinking sheet. The numerical solution for a MHD boundary layer and heat flow past a stretching surface inserted in a non-Darcy spongy medium with fluid-particle suspension was found by Gireesha *et al.* [33]. Currently a stability analysis of boundary layer flow and heat transfer through permeable surface which is itself embedded in a porous medium was given by Yasin *et al.* [34] numerically. Momentum and thermal boundary layer for a porous cylinder was reported by Sia *et al.* [35].

The theme of the current article is to offer a numerical solution of Williamson time-dependent fluid flow due to a porous stretching surface. Thus an attempt is performed by using theoretical grounds. Moreover, the effects of magnetic field are also taken into account. The nano sized particles are assumed to be suspended in the flow regime. The obtained results are provided with the aid of both graphs and tables shooting method [36–38]. The results are compared with the existing literature in a limiting sense which yields the surety of the present work.

2 Mathematical formulation

The constitutive equation for the Williamson fluid model is defined by the form

$$\mathbf{T} = -p\mathbf{I} + \tau, \tag{1}$$

where

$$\tau = \left[\mu_\infty + \frac{(\mu_0 - \mu_\infty)}{1 - \Gamma\dot{\gamma}}\right] \mathbf{A_1}. \tag{2}$$

here p, $\mathbf{I}$ and τ are the pressure, identity vector and extra stress tensor. Γ is a positive time constant, *i.e.*, $\Gamma > 0$. μ_0 is the low shear rate viscosity, μ_∞ is the high shear rate viscosity, $\mathbf{A_1}$ is the first Rivlin-Ericksen tensor and shear rate $\dot{\gamma}$ is defined as

$$\dot{\gamma} = \sqrt{\frac{1}{2}\pi}, \tag{3}$$

where

$$\pi = \frac{1}{2}\,\mathrm{trace}(\mathbf{A_1}^2). \tag{4}$$

Here we consider only the case for $\mu_\infty = 0$ and $\Gamma\dot{\gamma} < 1$. Now the extra stress tensor reduced to

$$\tau = \left[\frac{\mu_0}{1 - \Gamma\dot{\gamma}}\right] \mathbf{A_1}. \tag{5}$$

By applying binomial expansion to eq. (5) one one can obtain the following expressions:

$$\tau = \mu_0[1 + \Gamma\dot{\gamma}]A_1, \tag{6}$$

$$\dot{\gamma} = \left[\left(\frac{\partial u}{\partial x}\right)^2 + \frac{1}{2}\left(\frac{\partial u}{\partial y} + \frac{\partial v}{\partial x}\right)^2 + \left(\frac{\partial v}{\partial y}\right)^2\right]^{\frac{1}{2}}, \tag{7}$$

$$\tau_{xx} = 2\mu_0[1 + \Gamma\dot{\gamma}]\left(\frac{\partial u}{\partial x}\right), \tag{8}$$

$$\tau_{xy} = \mu_0[1 + \Gamma\dot{\gamma}]\left(\frac{\partial u}{\partial y} + \frac{\partial v}{\partial x}\right), \tag{9}$$

$$\tau_{yy} = 2\mu_0[1 + \Gamma\dot{\gamma}]\left(\frac{v}{y}\right), \tag{10}$$

$$\tau_{xz} = \tau_{yz} = \tau_{zx} = \tau_{zy} = \tau_{zz} = 0. \tag{11}$$

The component form of continuity and momentum equations can be defined as

$$\frac{\partial u}{\partial x} + \frac{\partial v}{\partial y} = 0, \tag{12}$$

$$\rho\left(\frac{\partial u}{\partial t} + u\frac{\partial u}{\partial x} + v\frac{\partial u}{\partial y}\right) = -\frac{\partial p}{\partial x} + \frac{\partial}{\partial x}(\tau_{xx}) + \frac{\partial}{\partial y}(\tau_{xy}), \tag{13}$$

$$\rho\left(\frac{\partial v}{\partial t} + u\frac{\partial v}{\partial x} + v\frac{\partial v}{\partial y}\right) = -\frac{\partial p}{\partial y} + \frac{\partial}{\partial x}(\tau_{yx}) + \frac{\partial}{\partial y}(\tau_{yy}), \tag{14}$$

where $u(x, y, t)$ and $v(x, y, t)$ are the velocity components along the flow direction and normal to the flow direction, respectively. The boundary layer approximations with zero pressure gradient assumption reduce the momentum, energy and nanoparticle concentration equations to

$$\frac{\partial u}{\partial x} + \frac{\partial v}{\partial y} = 0, \tag{15}$$

$$\frac{\partial u}{\partial t} + u\frac{\partial u}{\partial x} + v\frac{\partial u}{\partial y} = \nu\left[\frac{\partial^2 u}{\partial y^2} + \sqrt{2}\Gamma\frac{\partial u}{\partial y}\frac{\partial^2 u}{\partial y^2}\right] - \frac{\sigma B^2(t)u}{\rho}, \tag{16}$$

$$\frac{\partial T}{\partial t} + u\frac{\partial T}{\partial x} + v\frac{\partial T}{\partial y} = \alpha_m\frac{\partial^2 T}{\partial y^2} + \tau\left[D_B\frac{\partial C}{\partial y}\frac{\partial T}{\partial y} + \frac{D_T}{D_\infty}\left(\frac{\partial T}{\partial y}\right)^2\right], \tag{17}$$

$$\frac{\partial C}{\partial t} + u\frac{\partial C}{\partial x} + v\frac{\partial C}{\partial y} = D_B\frac{\partial^2 C}{\partial y^2} + \frac{D_T}{D_\infty}\frac{\partial^2 T}{\partial y^2}, \tag{18}$$

their respective boundary conditions are

$$\begin{aligned} &u = U_w(x, t), \qquad v = V_w(t), \qquad T = T_w(x, t), \\ &C = C_w(x, t), \quad \text{at } y = 0, \end{aligned} \tag{19}$$

$$u \to 0, \quad T \to T_\infty, \quad C \to C_\infty, \quad \text{when } y \to \infty. \tag{20}$$

In the above equations ν represents the kinematic viscosity, $\tau = \frac{(\rho c)_p}{(\rho c)_f}$ defines the ratio of effective heat capacity of the nanoparticles to the effective heat capacity of the base fluid. Both D_T and D_B are the coefficients of thermophoresis diffusion and Brownian diffusion, respectively. T is the fluid temperature and C is the nanoparticle concentration. The assumed forms of stretching velocity, surface temperature, mass fluid velocity, surface nanoparticle concentration and magnetic field are given as follows:

$$\begin{aligned} U_w(x, t) &= \frac{ax}{1 - ct}, \qquad T_w(x.t) = T_\infty + \frac{T_0 U_w x}{\nu(1 - ct)^{\frac{1}{2}}}, \\ V_w(t) &= \frac{-V_0}{(1 - ct)^{\frac{1}{2}}}, \qquad C_w(x, t) = C_\infty + \frac{C_0 U_w x}{\nu(1 - ct)^{\frac{1}{2}}}, \qquad B(t) = \frac{B_0}{(1 - ct)^{\frac{1}{2}}}, \end{aligned} \tag{21}$$

where a and c are positive constants with unit of s^{-1} or to balance the dimensions with $(\text{time})^{-1}$ and it is certain that $1 - ct > 0$. B_0 is the magnetic field intensity and V_0 is the uniform suction/injection velocity. One can introduce

a stream function ψ which satisfies the continuity equation, such that

$$u = \frac{\partial \psi}{\partial y}, \qquad v = -\frac{\partial \psi}{\partial x}. \tag{22}$$

The set of transformations for order reduction can be defined as

$$\eta = y\sqrt{\frac{U_w}{\nu x}}, \qquad \psi = \sqrt{U_w \nu x} f(\eta), \tag{23}$$

$$\theta = \frac{T - T_\infty}{T_w - T_\infty}, \qquad \phi = \frac{C - C_\infty}{C_w - C_\infty}. \tag{24}$$

By using eqs. (22)–(24) into eqs. (16)–(20) one can obtain

$$f'''[1 + Wef''] + ff'' - f'^2 - A\left[f' + \frac{\eta}{2}f''\right] - M^2 f' = 0, \tag{25}$$

$$\theta'' + Pr(f\theta' - 2f'\theta) - Pr\frac{A}{2}(\eta\theta' + 3\theta) + Pr\left[Nb\theta'\phi' + Nt(\theta')^2\right] = 0, \tag{26}$$

$$\phi'' + PrLe(f\phi' - 2f'\phi) - Pr\frac{A}{2}Le(\eta\phi' + 3\phi) + \frac{Nt}{Nb}\theta'' = 0, \tag{27}$$

along with the boundary conditions

$$f(0) = s, \qquad f'(0) = 1, \qquad \theta(0) = 1, \qquad \phi(0) = 1, \tag{28}$$

$$f' \to 0, \quad \theta \to 0, \quad \phi \to 0, \quad \text{at } \eta \to \infty. \tag{29}$$

Here differentiation is with respect to η. The dimensionless numbers We, A, M and Pr, Nb, Nt, Le and s are the Weissenberg number, the unsteadiness parameter, the magnetic parameter, the Prandtl number, the Brownian motion parameter, the thermophoresis parameter, the Lewis number and the mass transfer parameter $s > 0$ for suction and $s < 0$ for injection. They are defined below

$$We = \sqrt{\frac{a^3 \Gamma x^2}{\nu(1-ct)^3}}, \qquad A = \frac{c}{a}, \qquad M = \sqrt{\frac{\sigma}{\rho a}}B_0,$$
$$Pr = \frac{\mu C_p}{k}, \qquad Nb = \frac{\tau D_B (C_w - C_\infty)}{\nu},$$
$$Nt = \frac{\tau D_T (T_w - T_\infty)}{\nu T_\infty}, \qquad Le = \frac{\alpha_m}{D_B}, \qquad s = \frac{v_0}{\sqrt{\nu a}}. \tag{30}$$

3 Skin friction coefficient, local Nusselt number and local Sherwood number

The skin friction coefficient is defined below

$$C_f = \frac{\tau_w}{\frac{1}{2}\rho U_w^2}, \tag{31}$$

in the above expression τ_w represents the shear stress at the permeable surface. For the Williamson fluid surface the shear stress is defined as

$$\tau_w = \mu_0 \left[\frac{\partial u}{\partial y} + \frac{\Gamma}{\sqrt{2}}\left(\frac{\partial u}{\partial y}\right)^2\right]_{y=0}, \tag{32}$$

after incorporating the eq. (32) into eq. (31), one has the following expression:

$$\frac{C_f Re_x^{\frac{1}{2}}}{2} = f''(0) + \frac{We}{2}f''^2(0). \tag{33}$$

The local Nusselt number can be written as

$$Nu_x = \frac{x q_w}{k(T_w - T_\infty)}, \tag{34}$$

where q_w is the measure of heat transfer at the surface of a permeable stretching sheet and defined as

$$q_w = -k\left(\frac{\partial T}{\partial r}\right)_{r=R}. \tag{35}$$

Using eq. (33) into eq. (32) one has

$$Nu_x Re_x^{-\frac{1}{2}} = -\theta'(0). \tag{36}$$

The Sherwood number is defined as

$$Sh_x = \frac{xq_m}{D_B(C_w - C_\infty)}, \tag{37}$$

where

$$q_m = -D_B\left(\frac{\partial C}{\partial y}\right)_y = 0, \tag{38}$$

by using eq. (38) into eq. (37) one can get

$$Re^{-\frac{1}{2}} Sh_x = -\phi'(0), \tag{39}$$

where $Re_x = \frac{Ux}{\nu}$ denotes the Reynolds number.

4 Method of solution

The system given by eqs. (25)–(27) is non-linear and it is difficult to find out the closed form solution, therefore as a numerical solution one can write

$$f''' = \frac{f'^2 - ff'' + A(f' + \frac{\eta}{2}) + M^2 f'}{1 + Wef''}, \tag{40}$$

$$\theta'' = Pr\frac{A}{2}(\eta\theta' + 3\theta) - Pr\left[f\theta' - 2f'\theta - Pr(Nb\theta'\phi' + Nt(\theta')^2)\right], \tag{41}$$

$$\phi'' = Pr\frac{A}{2}Le(\eta\phi' + 3\phi) - PrLe(f\phi' - 2f'\phi) - \frac{Nt}{Nb}\theta'', \tag{42}$$

to implement the shooting method we have introduced dummy variables as follows:

$$\begin{aligned} &f = y_1, \quad f' = y_2, \quad f'' = y_3, \quad f''' = y_3', \\ &\theta = y_4, \quad \theta' = y_5, \quad \theta'' = y_5', \\ &\phi = y_6, \quad \phi' = y_7, \quad \phi'' = y_7'. \end{aligned} \tag{43}$$

The equivalent form of eqs. (25)–(27) in terms of initial value problem can be written as

$$y_1' = y_2, \tag{44}$$

$$y_2' = y_3, \tag{45}$$

$$y_3' = \frac{y_2^2 + A(y_2 + \frac{\eta}{2}y_3) - y_1y_3 + M^2y_2}{1 + Wey_3}, \tag{46}$$

$$y_4' = y_5, \tag{47}$$

$$y_5' = -Pr(y_1y_5 - 2y_2y_4) + Pr\frac{A}{2}(\eta y_5 + 3y_4) - Pr[Nby_5y_7 + Nt(y_5)^2], \tag{48}$$

$$y_6' = y_7, \tag{49}$$

$$y_7' = Pr\frac{A}{2}Le(\eta y_7 + 3y_6) - PrLe(y_1y_7 - 2y_2y_6) - \frac{Nt}{Nb}y_5'. \tag{50}$$

The reduced endpoint conditions are

$$\begin{aligned} &y_1(0) = s, \quad y_2(0) = 1, \quad y_3(0) = a_1, \quad y_4(0) = 1, \\ &y_5(0) = a_2, \quad y_6(0) = 1, \quad y_7(0) = a_3. \end{aligned} \tag{51}$$

where a_1, a_2 and a_3 are initial guessed values.

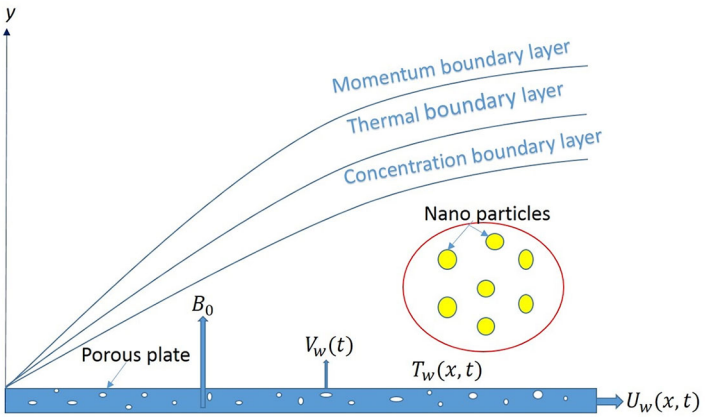

Fig. 1. Physical model.

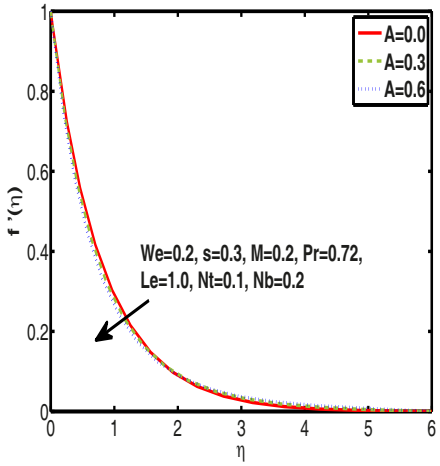

Fig. 2. Impact of unsteadiness parameter A on velocity profile.

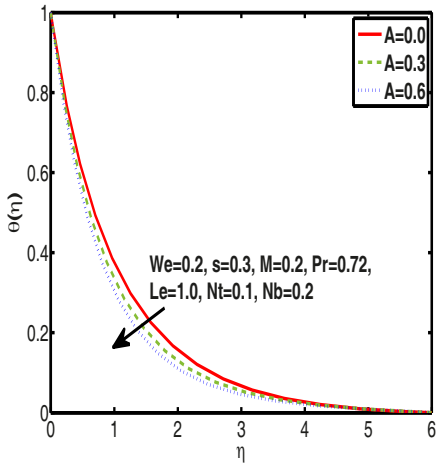

Fig. 3. Impact of unsteadiness parameter A on temperature profile.

5 Results and discussions

The outcomes by means of the shooting method are reported through both tables and figures. Figure 1 is the geometric representation of the flow problem. In detail, figs. 2–4 exhibit that there is a decrease in velocity, temperature and concentration to be more specific in unsteadiness parameter. Figure 2 depicts that the momentum boundary layer decreases with increase in unsteadiness parameter A. When the unsteadiness parameters increase the fluid temperature decreases due to a rapid transfer of heat through the permeable sheet. A similar trend is

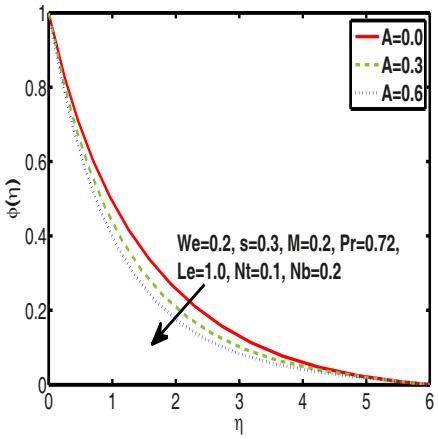

Fig. 4. Impact of unsteadiness parameter A on nanoparticle concentration profile.

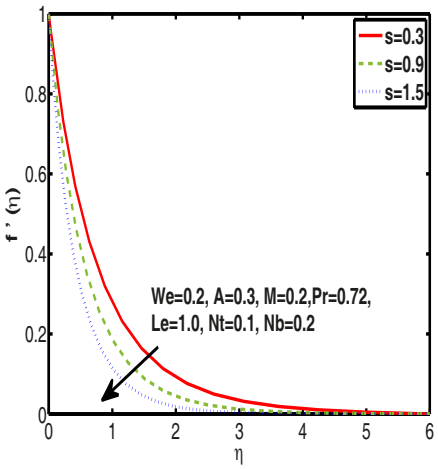

Fig. 5. Impact of mass transfer parameter s on velocity profile.

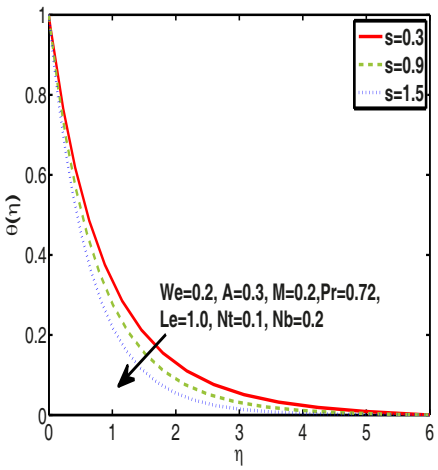

Fig. 6. Impact of mass transfer parameter s on temperature profile.

noticed for nanoparticle concentration via unsteadiness parameter as shown in fig. 4. Figures 5–7 are plotted to examine the effect of mass transfer parameters on fluid velocity, temperature and nanoparticle concentration respectively. It is noticed that fluid velocity, temperature and nanoparticle concentration are a decreasing function of the mass transfer parameter that an increase in the mass transfer parameter brings declined curves in velocity, temperature and nanoparticle concentration. Figures 8 and 9 provide the impact of a magnetic field parameter

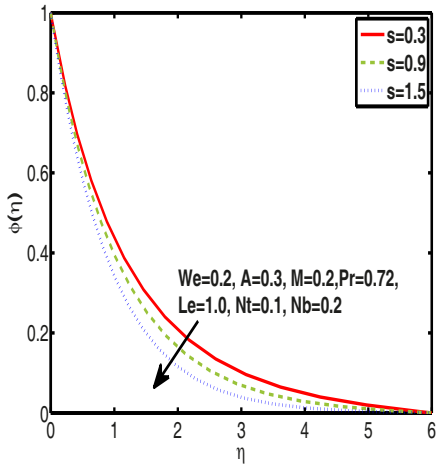

Fig. 7. Impact of mass transfer parameter s on concentration profile.

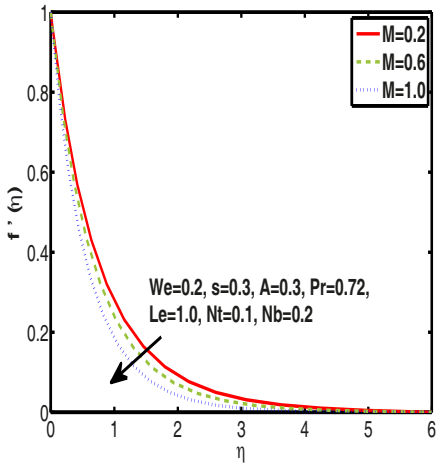

Fig. 8. Impact of magnetic parameter M on velocity profile.

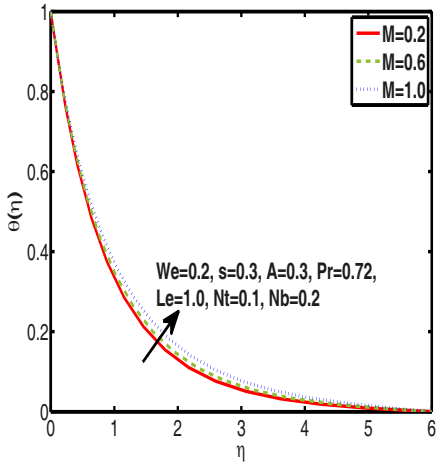

Fig. 9. Impact of magnetic parameter M on temperature profile.

on both fluid velocity and temperature distributions. It is observed that the velocity profile is a decreasing function of magnetic field parameter M. When the magnetic field parameter increases the magnitude of the Lorentz force increases. Hence large resistance is forced by fluid particles and as a result the velocity of the fluid decreases. In parallel context due to large resistance heat is produced which enhances the temperature of the fluid. Figure 10 is used to examine the impact of the Weissenberg number on the velocity profile. It is noticed that the velocity profile is a

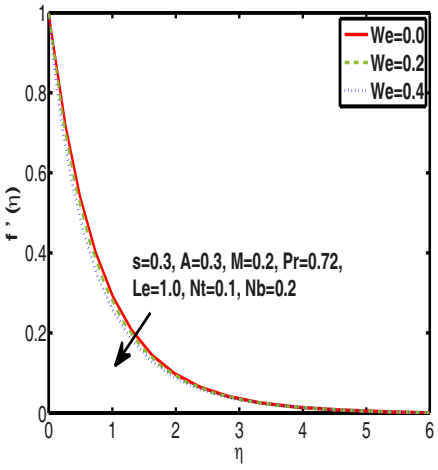

Fig. 10. Impact of Weissenberg number We on velocity profile.

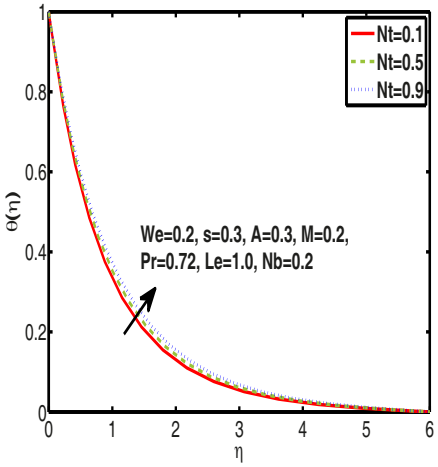

Fig. 11. Impact of thermophoresis parameter Nt on temperature profile.

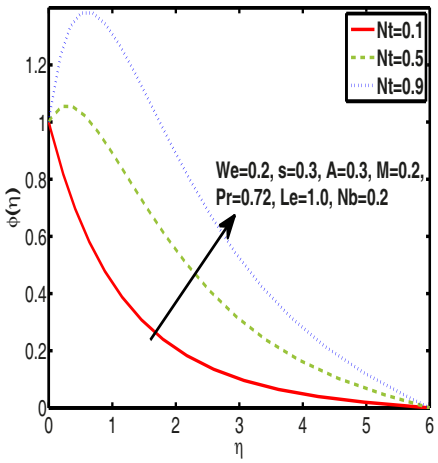

Fig. 12. Impact of thermophoresis parameter Nt on concentration profile.

decreasing function of the Weissenberg number. The Weissenberg number is the ratio of relaxation time to retardation time. Therefore an increase in relaxation time confirms the dominance of viscous forces as a result velocity curves show declining values. The impact of the thermophoresis parameter on both temperature and nanoparticle concentration is tested in figs. 11 and 12.

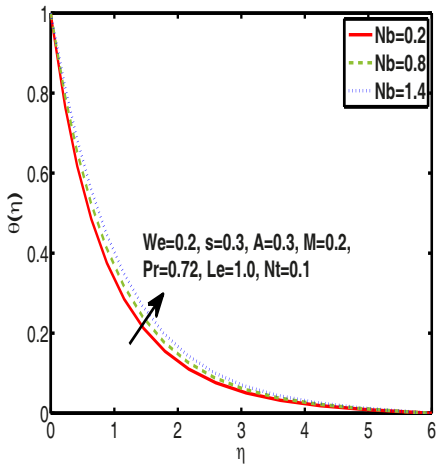

Fig. 13. Impact of Brownian motion parameter Nb on temperature profile.

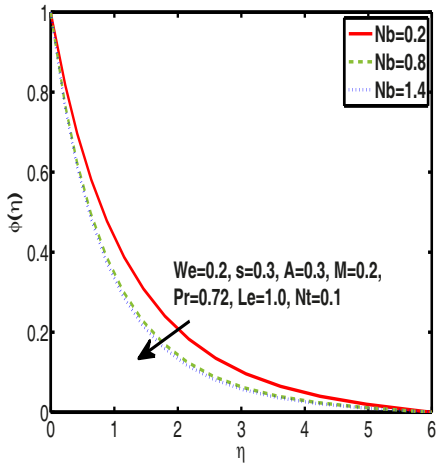

Fig. 14. Impact of Brownian motion parameter Nt on concentration profile.

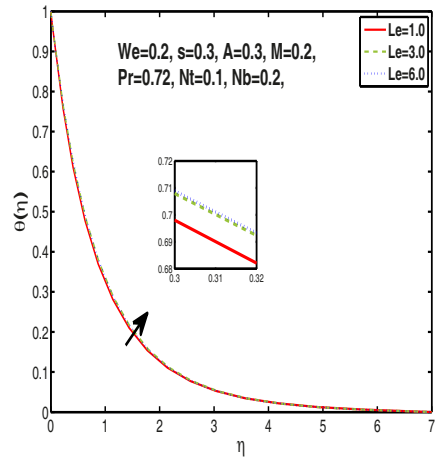

Fig. 15. Impact of Lewis number Le on temperature profile.

It is clear from the figures that by increasing the values of the thermophoresis parameter both temperature and nanoparticle concentration show increasing values. Figures 13 and 14 reveal the effect of the dimensionless Brownian motion parameter on the thermal and concentration boundary layer. By definition the Brownian motion parameter increases the kinetic energy of the nanoparticles due to which the temperature of the nanofluid increases. In result of this motion the thermal boundary layer thickness increases.

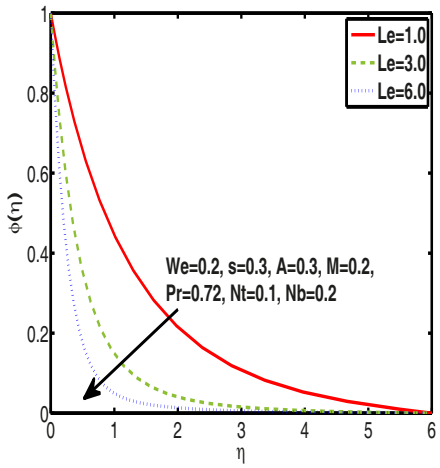

Fig. 16. Impact of Lewis number Le on concentration profile.

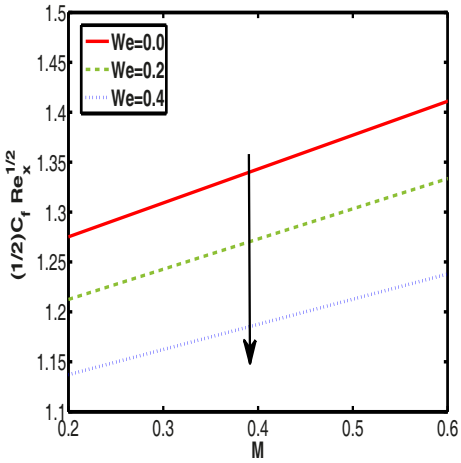

Fig. 17. Skin friction variation due to a change in magnetic parameter M and Weissenberg parameter We.

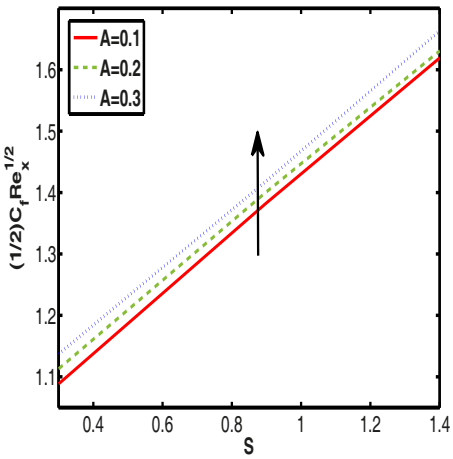

Fig. 18. Skin friction variation due to a change in unsteadiness parameter A and mass transfer parameter s.

The increase in kinetic energy is the cause of dispersion of nanoparticles which declines the concentration boundary layer thickness of nanofluids. Figure 15 shows the impact of the Lewis number on the temperature profile minutely. The Lewis number has a direct relation with the thermal diffusion so an increment in the Lewis number enhances the heat transfer, and as a result temperature increases. Figure 16 reports the impact of the Lewis number on the concentration profile. The nanoparticle concentration is a decreasing function of the Lewis number. Figure 17 reveals

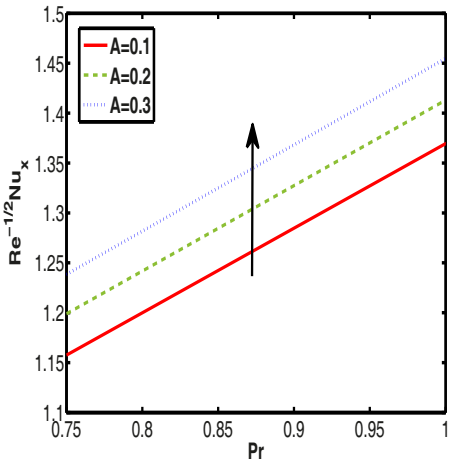

Fig. 19. Local Nusselt number variation due to a change in unsteadiness parameter A and Prandtl number Pr.

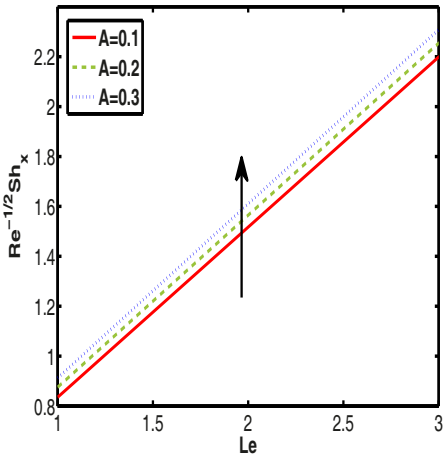

Fig. 20. Sherwood number variation due to a change in unsteadiness parameter A and Lewis number Le.

Table 1. Comparison of skin friction $-f''(0)$ with previously published data considering unsteadiness parameter variation A when $M = s = We = 0$.

A	Khan and Azam [39]	Present results
0.0	1.0000	1.0005
0.2	1.06801	1.0685
0.4	1.13469	1.1349
0.6	1.19912	1.1992

the results due to friction offered by the stretching permeable surface. It clarifies an increase in the skin friction coefficient due to an increase in the magnetic parameter. But there is a decline in $(1/2)Re_x^{1/2}C_f$ by incrementing the Weissenberg number. Figure 18 reports the influence of both the unsteadiness parameter and the mass transfer parameter on the skin friction coefficient. The influence of the unsteadiness parameter on both local Nusselt number and local Sherwood number is examined and provided by figs. 19 and 20, respectively. It is seen that both local Nusselt number and local Sherwood number are an increasing function of unsteadiness parameter A. Moreover it is also clear from the figures that the local Nusselt and Sherwood numbers reflect increasing values towards higher values of the Prandtl and Lewis numbers, respectively. Table 1 is constructed to provide the comparison of our work with the existing literature. It is observed that they have an excellent match with Khan *et al.* [39]. Table 2 indicates the effect of non-dimensional parameters upon skin friction coefficient $(f''(0) + \frac{We}{\sqrt{2}}f''^2(0))$. The values in the table show an enhancement in the local skin friction due to an increase in unsteadiness parameter A, mass transfer s and magnetic parameter M but it drops due to an increment in Weissenberg number We. Table 3 reports the effects of the

Table 2. Numerically computed value of skin friction for different values of A, M, s and We.

A	M	s	We	$\frac{1}{2}C_f Re_x{}^{\frac{1}{2}}$
0.0	0.2	0.3	0.2	1.0005
0.1	–	–	–	1.08854
0.2	–	–	–	1.11305
0.3	–	–	–	1.13710
–	0.6	–	–	1.23785
–	1.0	–	–	1.90526
–	0.2	0.9	–	1.41889
–	–	1.5	–	1.68579
–	–	0.3	0.0	1.2752
–	–	–	0.2	1.13711
–	–	–	0.4	0.88380

Table 3. Numerically computed values of the Nusselt number for different values of A, Pr, Nt, Nb and Le by fixing $s = 0.3$ and $M = We = 0.2$.

A	Pr	Nt	Nb	Le	$Re^{1/2}Nu_x$
0.0	0.72	0.1	0.2	1.0	1.0883
0.1	–	–	–	–	1.1321
0.2	–	–	–	–	1.1733
0.3	–	–	–	–	1.2125
–	1.00	–	–	–	1.4548
–	1.30	–	–	–	1.6671
–	0.72	0.5	–	–	1.1489
–	–	0.9	–	–	1.0915
–	–	0.1	0.8	–	1.0467
–	–	–	1.4	–	0.9051
–	–	–	0.2	3.0	1.1781
–	–	–	–	6.0	1.1575

Table 4. Numerically computed values of the Sherwood number for different values of A, Pr, Nt, Nb and Le by fixing $s = 0.3$ and $M = We = 0.2$.

A	Pr	Nt	Nb	Le	$Re^{-1/2}Sh_x$
0.0	0.72	0.1	0.2	1.0	0.7915
0.1	–	–	–	–	0.8353
0.2	–	–	–	–	0.8755
0.3	–	–	–	–	0.9128
–	1.00	–	–	–	1.1455
–	1.30	–	–	–	1.3767
–	0.72	0.5	–	–	0.4744
–	–	0.9	–	–	1.6819
–	–	0.1	0.8	–	1.2146
–	–	–	1.4	–	1.2561
–	–	–	0.2	3.0	2.3083
–	–	–	–	6.0	3.7891

non-dimensional parameter on local Nusselt number $-\theta'(0)$. The result implies that the Nusselt number increases with the increase in unsteadiness parameter A and Prandtl number Pr but the increment of thermophoresis parameter Nt, Brownian motion parameter Nb and Lewis number Le reduces the local Nusselt number. Also it fixes the values of the rest of the parameters. Table 4 uncovers the impact of non-dimensional parameters towards the local Sherwood number $-\phi'(0)$. For the controlled values of s, M and We there is an increase in the Sherwood number by the increase in unsteadiness parameter A, Prandtl number Pr, Lewis number Le and Brownian motion parameter Nb. But the enhancement of the thermophoresis parameter Nt reduces the local Sherwood number.

6 Concluding remarks

- The Williamson fluid velocity, temperature and nanoparticles concentrations are a decreasing function of the unsteady parameter.
- The fluid velocity, temperature and nanoparticle concentration reflect declining curves for the mass transfer parameter.
- The velocity profile shows a declining nature towards the magnetic field parameter but the opposite trend is noticed for the case temperature profile.
- Both temperature and nanoparticles concentration show increasing values via thermophoresis parameter.
- The skin friction coefficient increases for the positive values of both mass transfer parameter and unsteadiness parameter.
- The Nusselt number shows higher values for the increasing values of both Prandtl number and unsteadiness parameter.

Nomenclature

(x, y)	Space variables	τ	Extra stress tensor
Γ	Time material constant	μ	Dynamic viscosity
u	Component of velocity along the x-direction	μ_0	Zero shear rate viscosity
v	Component of velocity along the y-direction	μ_∞	Infinite shear rate viscosity
t	Time	$\dot{\gamma}$	Shear rate
T	Fluid temperature	η	Variable of local similarity
C	Nanoparticle concentration	ψ	Stream function
p	Pressure	ρ	Fluid density
$\mathbf{I}$	Identity tensor	ν	Kinematic viscosity
f'	Non-dimensionalized velocity	θ	Non-dimensionalized temperature
We	Weissenberg number	ϕ	Non-dimensionalized concentration
M	Magnetic parameter	α_m	Effective thermal diffusivity
Pr	Prandtl number	q_w	Wall heat flux
s	Mass transfer parameter	q_m	Wall mass flux
Re	Reynolds number	U_m	Stretching velocity
A_1	First Rivlin-Ericksen tensor	T_w	Surface/wall temperature
$B(t)$	Unsteady magnetic field	C_w	Surface/wall nanoparticle concentration
B_0	Magnitude of magnetic field	V_w	Mass fluid velocity
A	unsteadiness parameter	τ_w	Wall shear stress
Le	Lewis number	C_p	Specific heat capacity
Nb	Brownian motion parameter	D_T	Coefficient of thermophoresis diffusion
Nt	Thermophoresis parameter	D_B	Coefficient of Brownian diffusion
V_0	Uniform suction/injection velocity	C_∞	Ambient concentration
a, c	Positive constants	T_∞	Ambient temperature
k	Thermal conductivity	C_{fx}	Local skin friction
T_0	Reference temperature	Nu_x	Local Nusselt number
C_0	Reference concentration	Sh_x	Local Sherwood number

References

1. R.A. Damseh, Int. J. Appl. Mech. Eng. **11**, 289 (2006).
2. M.S. Abel, M.M. Nandeppanavar, Commun. Nonlinear Sci. Numer. Simul. **14**, 2120 (2009).
3. J.H. Merkin, V. Kumaran, Eur. J. Mech. B/Fluids **29**, 357 (2010).
4. M.M. Nandeppanavar, K. Vajravelu, M.S. Abel, Commun. Nonlinear Sci. Numer. Simul. **16**, 3578 (2011).
5. R.B. Kudenatti, S.R. Kirsur, L.N. Achala, N.M. Bujurke, Commun. Nonlinear Sci. Numer. Simul. **18**, 1151 (2013).
6. W.A. Khan, O.D. Makinde, Z.H. Khan, Int. J. Heat Mass Transfer **74**, 285 (2014).
7. F. Mabood, W.A. Khan, A.I.M. Ismail, J. Magn. & Magn. Mater. **374**, 569 (2015).
8. M. Khan, M. Hussain, M. Azam, J. Magn. & Magn. Mater. **412**, 63 (2016).
9. K.U. Rehman, M.Y. Malik, O.D. Makinde, A.A. Malik, Eur. Phys. J. Plus **132**, 427 (2017).
10. M. Khan, A.S. Alshomran, J. Magn. & Magn. Mater. **443**, 13 (2017).
11. M.Y. Malik, S. Bilal, M. Bibi, Results Phys. **7**, 482 (2017).
12. M. Khan, J. Taiwan Inst. Chem. Eng. **77**, 282 (2017).
13. M.Y. Malik, S. Bilal, M. Bibi, U. Ali, Results Phys. **7**, 544 (2017).
14. K.U. Rehman, Aqeela Qaiser, M.Y. Malik, U. Ali, Chin. J. Phys. **55**, 1605 (2017).
15. K. Stewarston, Adv. Appl. Mech. **6**, 1 (1960).
16. B.V. Perepelitza, Exp. Therm. Fluid Sci. **6**, 348 (1993).
17. N. Bachok, A. Ishak, I. Pop, Int. J. Heat Mass Transfer **55**, 2102 (2012).
18. D. Andrew, S. Rees, A. Bassom, Int. J. Heat Mass Transfer **93**, 1100 (2016).
19. R.V. Williamson, Ind. Eng. Chem. Res. **11**, 1108 (1929).
20. Dapra, G. Scarpi, Int. J. Rock Mech. Min. Sci. **44**, 271 (2007).
21. N.A. Khan, S. Khan, F. Riaz, Math. Sci. Lett. **3**, 199 (2014).
22. T. Hayat, Shahida bibi, M. Rafiq, A. Alsaedi, F.M. Abbasi, J. Magn. & Magn Mater. **401**, 733 (2016).
23. M.Y. Malik, M. Bibi, F. Khan, T. Salahuddin, AIP Adv. **6**, 035101 (2016).
24. K.U. Rehman, A.A. Khan, M.Y. Malik, U. Ali, M. Naseer, Chin. J. Phys. **55**, 1637 (2017).
25. K.U. Rehman, A.A. Khan, M.Y. Malik, U. Ali, Methods X **4**, 429 (2017).
26. S.U.S. Choi, J.A. Eastman, in *Proceedings of the 1995 ASME International Mechanical Engineering Congress & Exposition* (San Francisco, 1995).
27. S.K. Nandy, T.R. Mahapatra, Int. J. Heat Mass Transfer **64**, 1091 (2013).
28. H. Shabgard, S. Kheradmand, H. Farzaneh, C. Bae, Appl. Therm. Eng. **110**, 244 (2017).
29. L.J. Crane, Z. Angew. Math. Phys. **21**, 645 (1970).
30. C.Y. Wang, Non-Linear Mech. **43**, 377 (2008).
31. T. Fang, S. Yao, J. Zhang, A. Aziz, Commun. Nonlinear Sci. Numer. Simul. **15**, 1831 (2010).
32. A. Ishak, L. Yian, I. Pop, Chem. Eng. Commun. **197**, 1417 (2010).
33. B.J. Gireesha, B. Mahanthesh, P.T. Manjunatha, R.S.R. Gorla, J. Niger. Math. Soc. **34**, 267 (2015).
34. M.H.M. Yasin, A. Ishak, I. Pop, Appl. Therm. Eng. **115**, 1407 (2017).
35. X. Sia, L. Lia, L. Zhenga, X. Zhangb, B. Liua, Comput. Fluids **105**, 280 (2014).
36. M.U. Rahman, M. Khan, Mehwish Manzur, Results Phys. **7**, 4364 (2017).
37. M. Awais, M.Y. Malik, Arif Hussain, T. Salahuddin, Eur. Phys. J. Plus **132**, 392 (2017).
38. M.U. Rahman, Mehwish Manzur, M. Khan, J. Mol. Liq. **223**, 217 (2016).
39. M. Khan, M. Azam, J. Mol. Liq. **225**, 554 (2017).